catalysts

MDPI

Article

Co-Promoted Ni Nanocatalysts Derived from NiCoAl-LDHs for Low Temperature CO_2 Methanation

Fanying Zhang [1], Bin Lu [2] and Peiqin Sun [1,*]

[1] Engineering Research Center of Advanced Functional Material Manufacturing of Ministry of Education, School of Chemical Engineering, Zhengzhou University, Zhengzhou 450000, China; fanyingzhang1@163.com
[2] (CNBM) Bengbu Design & Research Institute for Glass Industry Co., Ltd., Bengbu 233000, China; lubin@ctiec.net
* Correspondence: psun@zzu.edu.cn; Tel.: +86-0371-63887325

Abstract: Ni-based catalysts are prone to agglomeration and carbon deposition at high temperatures. Therefore, the development of Ni-based catalysts with high activities at low temperatures is a very urgent and challenging research topic. Herein, Ni-based nanocatalysts containing Co promoter with mosaic structure were prepared by reduction of NiCoAl-LDHs, and used for CO_2 methanation. When the reaction temperature is 250 °C (0.1 MPa, GHSV = 30,000 mL·g^{-1}·h^{-1}), the conversion of CO_2 on the $NiCo_{0.5}Al$-R catalyst reaches 81%. However, under the same test conditions, the conversion of CO_2 on the NiAl-R catalyst is only 26%. The low-temperature activity is significantly improved due to Co which can effectively control the size of the Ni particles, so that the catalyst contains more active sites. The CO_2-TPD results show that the Co can also regulate the number of moderately basic sites in the catalyst, which is beneficial to increase the amount of CO_2 adsorbed. More importantly, the $NiCo_{0.5}Al$-R catalyst still maintains high catalytic performance after 92 h of continuous reaction. This is due to the confinement effect of the AlO_x substrate inhibiting the agglomeration of Ni nanoparticles. The Ni-based catalysts with high performance at low temperature and high stability prepared by the method used have broad industrial application prospects.

Keywords: CO_2 methanation; low temperature; Co additive; NiCoAl-LDHs

Citation: Zhang, F.; Lu, B.; Sun, P. Co-Promoted Ni Nanocatalysts Derived from NiCoAl-LDHs for Low Temperature CO_2 Methanation. *Catalysts* **2021**, *11*, 121. https://doi.org/10.3390/catal11010121

Received: 23 December 2020
Accepted: 13 January 2021
Published: 15 January 2021

1. Introduction

The large amount of CO_2 emission has caused the greenhouse effect to be more obvious, consequently leading to serious environmental problems. Therefore, how to effectively reduce the concentration of CO_2 in the atmosphere has aroused widespread research interest [1–5]. At present, there have been many reports on the research in this aspect, such as the reduction of CO_2 to produce methanol [6,7], alkanes (CH_4, C_2H_6) [8–11] and alkenes (C_2H_4, C_3H_6, C_4H_8) [12–14]. Converting CO_2 into chemical products with high added value can not only reduce the concentration of CO_2 in the atmosphere but also realize the efficient recycling of resources. Among them, the production of CH_4 with CO_2 as a raw material can also help solve the problem of insufficient supply of CH_4 in the market, so the CO_2 methanation reaction has received increasing attention.

Although precious metal-based catalysts have excellent low-temperature catalytic activity [15,16], their cost is too high to be suitable for industrial applications. Compared with precious metal catalysts, Ni-based catalysts have poor low-temperature activity, but their cost is low [17–20]. Therefore, Ni-based catalysts are currently the most widely used in industry. However, the Ni-based catalysts currently used in industrial applications require relatively high activation temperatures [21,22]. As we know, CO_2 methanation is a strongly exothermic reaction, so high temperature is not conducive to the progress of the reaction. At the same time, when reacting at high temperatures, Ni-based catalysts are prone to agglomeration, sintering and carbon deposition, which may cause catalysts deactivation [23–25]. At present, the commonly used methods to improve the activity and

stability of Ni-based catalysts are the addition of additives (La, Pr, Mn, Fe) [26–28], carrier modification [24,29,30], restriction of the pore structure and so on [31,32]. Frontera et al. found that Gadolinia Doped Ceria support can generate more active oxygen vacancies, thereby significantly improving the catalytic performance of Ni-based catalysts in CO_2 methanation reaction [33]. In addition, the doped cerium oxide supported Ni-based catalysts can significantly improve the carbon deposition resistance and CO adsorption of the catalysts [34]. Although these methods have made some progress, the traditional supported Ni-based catalysts still have agglomeration and carbon deposition during the reaction process, and their low-temperature catalytic activity still needs to be further improved.

As a new type of layered nanomaterials, layered double hydroxides (LDHs) have adjustable metal cation types and ratios in their structure, so they are widely used in the field of heterogeneous catalysis [35–37]. For example, the Ni/Ru catalysts derived from hydrotalcites have excellent catalytic activity and stability in the CO_2 methanation reaction [38]. Hydrotalcites can not only be used as catalysts carriers but also as precursors for the direct preparation of catalysts. By changing the molar ratio of Ni to Fe in the hydrotalcites, the basic sites and particle size of the Ni-based catalysts can be adjusted, thereby improving the CO_2 methanation performance of the catalysts [39]. The metal catalysts prepared with hydrotalcites as the precursors have the advantages of high metal dispersion, small particle size and high activities. At the same time, the metal catalysts obtained by directly reducing the hydrotalcites will form a unique mosaic structure, thereby significantly improving the stability of metal nanoparticles [3,40]. Therefore, it is possible to use hydrotalcites as a precursor to prepare Ni-based catalysts with high low-temperature catalytic performance and high stability.

In this work, NiCoAl-LDH-derived Ni-based catalysts containing Co promoter were successfully prepared and used in low-temperature CO_2 methanation reactions. The promoter Co is beneficial to promote a reduction in Ni species, and can effectively control the size of Ni particles and the number of intermediate alkaline sites in the catalysts. Furthermore, the confinement effect of the AlO_x substrate can effectively inhibit the migration and agglomeration of Ni particles during the CO_2 methanation reaction, and improve the stability of the catalysts.

2. Results

2.1. Structural and Morphology Characterization of Samples

The XRD characterization technique was used to explore the phases of hydrothermally synthesized samples. As shown in Figure 1a, there are several diffraction peaks at 11.6°, 22.7°, 34.7°, 39.0°, 46.1°, 60.7° and 62.1°, which can be indexed to the (003), (006), (009), (015), (018), (110) and (113) crystal planes of typical LDHs, respectively [41]. The XRD results indicate that $NiCo_xAl$-LDHs (x = 0, 0.25, 0.5, 1) were successfully prepared. Compared with NiAl-LDH, the diffraction peak intensity of $NiCo_xAl$-LDHs became stronger, indicating that the addition of Co improves the crystallinity of hydrotalcites. The $NiCo_xAl$-LDHs precursors were directly reduced to prepare Co-promoted Ni-based catalysts, and the XRD results are shown in Figure 1b. It can be observed that the diffraction peaks of hydrotalcites disappeared, but new diffraction peaks appeared at 44.6°, 51.9°, 76.8°, which correspond to the (111), (200), (220) crystal planes of Ni [42]. This indicates that the phase transformation from the hydrotalcite precursor to the nickel-based catalyst was successfully achieved after hydrogen reduction treatment. The Ni particle sizes in the NiAl-R, $NiCo_{0.25}$Al-R, $NiCo_{0.5}$Al-R and $NiCo_1$Al-R catalysts calculated according to the Scherrer formula were 19.2, 16.6, 10.2 and 13.7 nm, respectively. This is attributed to the Co-promoter regulating effect on the size of Ni particles in the catalysts. The smaller the sizes of the Ni particles in the catalysts, the more active sites are exposed, which is crucial for improving the activity of the catalysts [43].

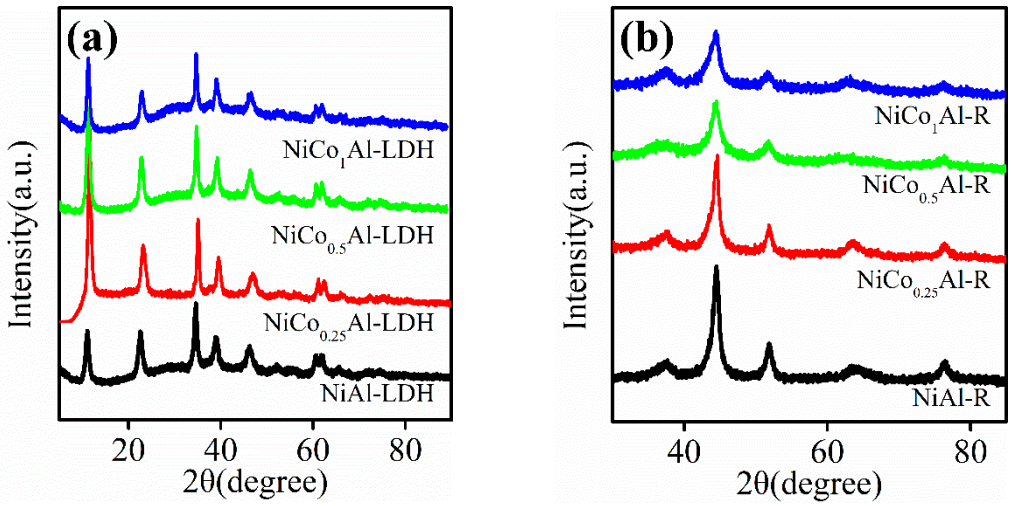

Figure 1. XRD profiles of $NiCo_xAl$-LDHs (**a**) and $NiCo_xAl$-R catalysts (**b**).

The N_2 adsorption–desorption isotherms and pore size distribution curves of the $NiCo_xAl$-R catalysts are shown in Figure 2. It can be seen from Figure 2a that NiAl-R catalyst is an IV type adsorption–desorption isotherm and type H1 hysteresis loop, which proves that the NiAl-R catalyst has a mesoporous structure and a narrow pore size distribution (shown in Figure 2b). When Co is added as a promoter, the $NiCo_xAl$-R catalysts are all type II adsorption–desorption isotherms and H3 type hysteresis loops, which indicates that there is a non-uniform slit pore structure in the $NiCo_xAl$-R catalysts. It can be clearly seen from Figure 2b that adding an appropriate amount of Co as a promoter can significantly increase the pore size in the $NiCo_xAl$-R catalysts, which is beneficial for the entry of feed gas (CO_2, H_2) and the escape of products (CO_2, CH_4, H_2).

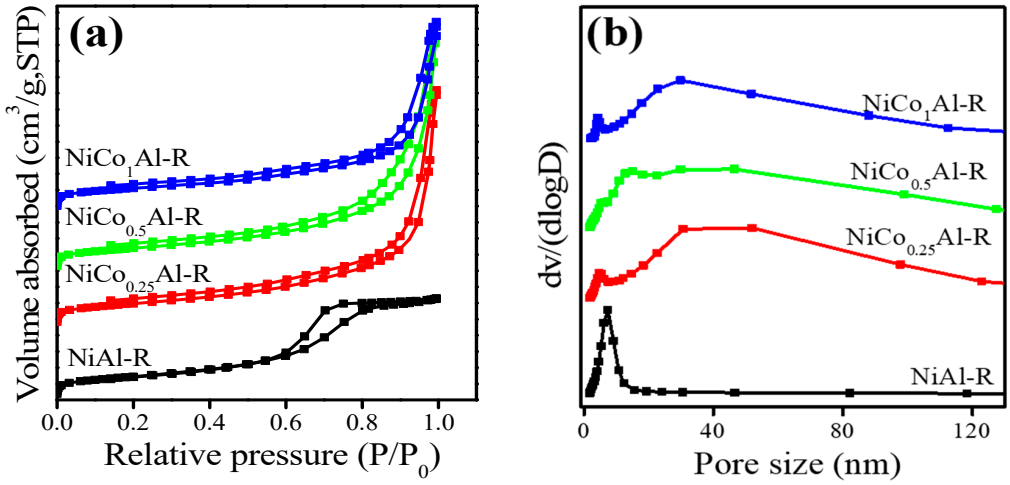

Figure 2. N_2 adsorption–desorption isotherms of $NiCo_xAl$-LDHs (**a**); pore size distribution curves of $NiCo_xAl$-R catalysts (**b**).

SEM characterization was used to explore the morphology of the $NiCo_xAl$-LDHs precursors and the $NiCo_xAl$-R catalysts (shown in Figure 3). According to the SEM characterization results, it is found that the prepared $NiCo_xAl$-LDHs precursors are all nanosheet structures and relatively uniform in size. Among them, the nanosheets in the NiAl-LDH precursor are relatively dispersed. However, the nanosheets in the $NiCo_xAl$-LDH precursors prepared after adding Co are intercalated and assembled to form a flower-like structure. Because the nanosheets are intercalated and stacked with each other, some irregular slit hole structures will be formed, which is consistent with the BET test results (shown

in Figure 2). In addition, SEM results show that the catalysts prepared by direct reduction of $NiCo_xAl$-LDH precursors are also a nanoplatelet structure (shown in Figure 3(a2–d2)), which is helpful for exploring the microstructure of the catalysts.

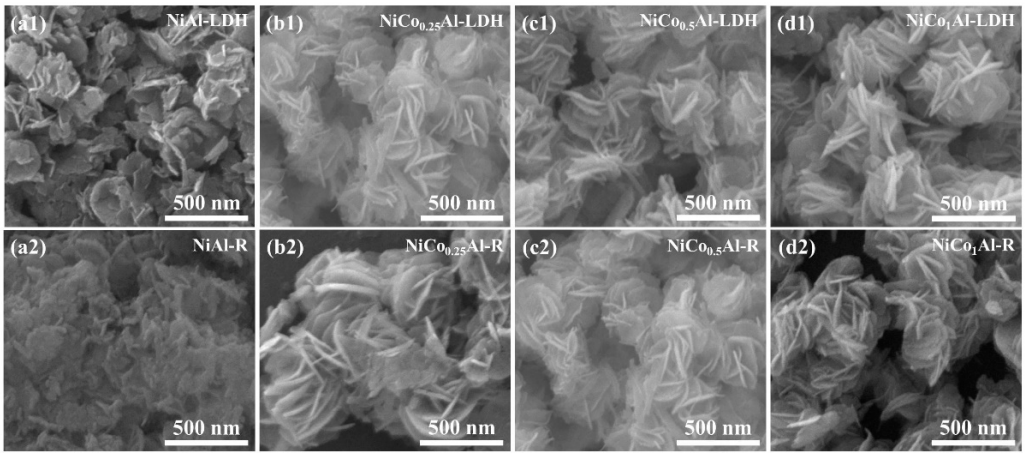

Figure 3. SEM micrographs of $NiCo_xAl$-LDHs: (**a1**) NiAl-LDH, (**b1**) $NiCo_{0.25}Al$-LDH, (**c1**) $NiCo_{0.5}Al$-LDH, (**d1**) $NiCo_1Al$-LDH and $NiCo_xAl$-R catalysts: (**a2**) NiAl-R, (**b2**) $NiCo_{0.25}Al$-R, (**c2**) $NiCo_{0.5}Al$-R, (**d2**) $NiCo_1Al$-R.

The H_2-TPR results of $NiCo_xAl$-LDHs precursors are shown in Figure 4. The NiAl-LDH sample has two obvious H_2 reduction signal peaks, and the corresponding center temperatures are 397 and 633 °C, respectively. The reduction peak at low temperature (397 °C) comes from the reduction in Ni species that interact weakly with the carrier, while the reduction peak at high temperature (633 °C) corresponds to the reduction in Ni species that interact strongly with the carrier [32]. Different from NiAl-LDH, $NiCo_{0.25}Al$-LDH, $NiCo_{0.5}Al$-LDH and $NiCo_1Al$-LDH all have three obvious reduction signal peaks, and the corresponding temperature ranges are 265–385 °C, 385–433 °C and 480–750 °C, respectively. By consulting the literature, it is found that the hydrogen signal peak in the range of 265–385 °C comes from the reduction in Co species [44–46]. It can be found from Figure 4 that as the Co content increases, the area of the corresponding reduction peak also gradually increases. In addition, the reduction peaks in the temperature range of 385–433 °C and 480–750 °C are derived from the reduction in Ni species. According to the H_2-TPR data, it is found that when the added amount of Co increases from 0 to 0.5 mmol, the reduction temperature required for Ni material decreases from 634 to 534 °C. However, when the amount of Co added continues to increase to 1 mmol, the reduction temperature required for Ni species increases from 534 to 631 °C. In summary, the Co additive can effectively regulate the interaction between the Ni substance and the supporter, so adding an appropriate amount of Co can significantly reduce the reduction temperature of the Ni species.

Since the basic sites on the catalyst surface play a vital role in the CO_2 hydrogenation reaction, it is necessary to study the distribution of basic sites on the catalyst surface by the CO_2-TPD data (shown in Figure 5). CO_2-TPD experiment results show that all catalysts contain two CO_2 desorption signal peaks; the corresponding temperature ranges are 65–195 °C and 205–450 °C, respectively. According to the reported literature, it can be observed that the two desorption signal peaks are derived from the CO_2 adsorbed at the weakly basic sites (surface OH^-) and the moderately basic sites (Lewis acid-based pairs), respectively [47]. Since the weakly basic sites have a weak adsorption force on CO_2, the adsorbed CO_2 is desorbed from the catalyst surface before it reacts, which is not conducive to the progress of the methanation reaction. Studies have shown that moderately basic sites have a strong adsorption force for CO_2 and a large amount of adsorption, which helps to improve the catalytic activity of the catalyst [48]. According to the results of CO_2-TPD, the relative content of intermediate basic sites in the catalysts is 68%, 80%, 88% and 77%,

respectively (shown in Table 1). According to the above results, it is found that the Co promoters can significantly increase the number of moderately basic sites in the catalysts, which is very important for improving the catalytic performance of the catalysts.

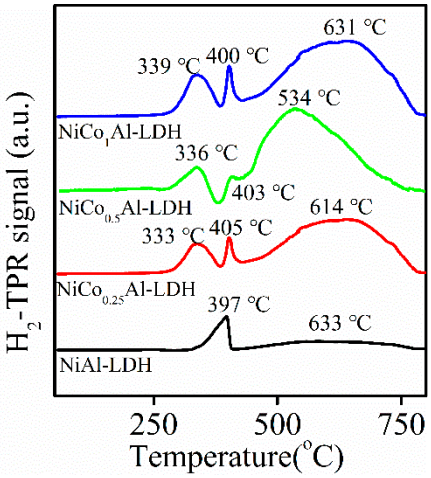

Figure 4. H_2-TPR profiles of the $NiCo_xAl$-LDHs.

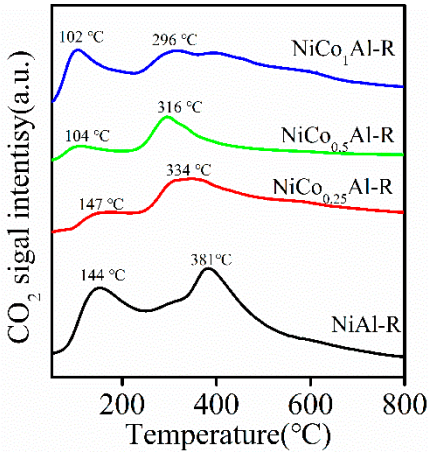

Figure 5. CO_2-TPD patterns of $NiCo_xAl$-R catalysts.

Table 1. Physical and chemical properties of $NiCo_xAl$-R samples.

Samples	[a] S_{BET} ($m^2 \cdot g^{-1}$)	[b] V_p ($m^3 \cdot g^{-1}$)	[c] Pore Diameter (nm)	[d] Basic Sites Percentage (%)	
				65 °C–195 °C	205 °C–450 °C
NiAl-R	116	0.2	5	32	68
$NiCo_{0.25}Al$-R	118	0.6	16	20	80
$NiCo_{0.5}Al$-R	117	0.5	16	14	86
$NiCo_1Al$-R	114	0.4	15	23	77

S_{BET} and V_p represent the specific surface area and pore volume of the catalysts. [a] Calculated by BET equation. [b] Measured by the volume of N_2 adsorbed at $p/p^0 = 0.97$. [c] Examined by BJH method. [d] Determined based on the CO_2-TPD results.

The microstructure of the prepared $NiCo_xAl$-R catalysts was further explored by TEM technology. The TEM characterization results further proved that the $NiCo_xAl$-R catalysts have a nanosheet structure, and the Ni nanoparticles are uniformly distributed in the substrate (shown in Figure 6a–d). The histogram in Figure 6 shows the size distribution of Ni nanoparticles in the $NiCo_xAl$-R catalysts. The average particle sizes of the Ni particles in the NiAl-R, $NiCo_{0.25}Al$-R, $NiCo_{0.5}Al$-R and $NiCo_1Al$-R catalysts measured by the TEM

test results are 19.3 ± 0.5 nm, 16.8 ± 0.5 nm and 10.1 ± 0.5, 13.6 ± 0.5 nm, respectively. This is consistent with the Ni particle size calculated from the XRD results (shown in Figure 1b). Figure 6e,f show high magnification TEM pictures of NiAl-R and $NiCo_{0.5}$Al-R, respectively. The lattice distance is 0.203 and 0.20 nm, corresponding to the (002) crystal plane of Co and the (111) crystal plane of Ni, respectively [49]. It can be seen from Figure 6e,f that both Ni nanoparticles and Co nanoparticles are embedded in the AlO_x substrate. This unique mosaic structure can effectively inhibit the migration and agglomeration of Ni nanoparticles, helping to improve the stability of the catalyst as a result.

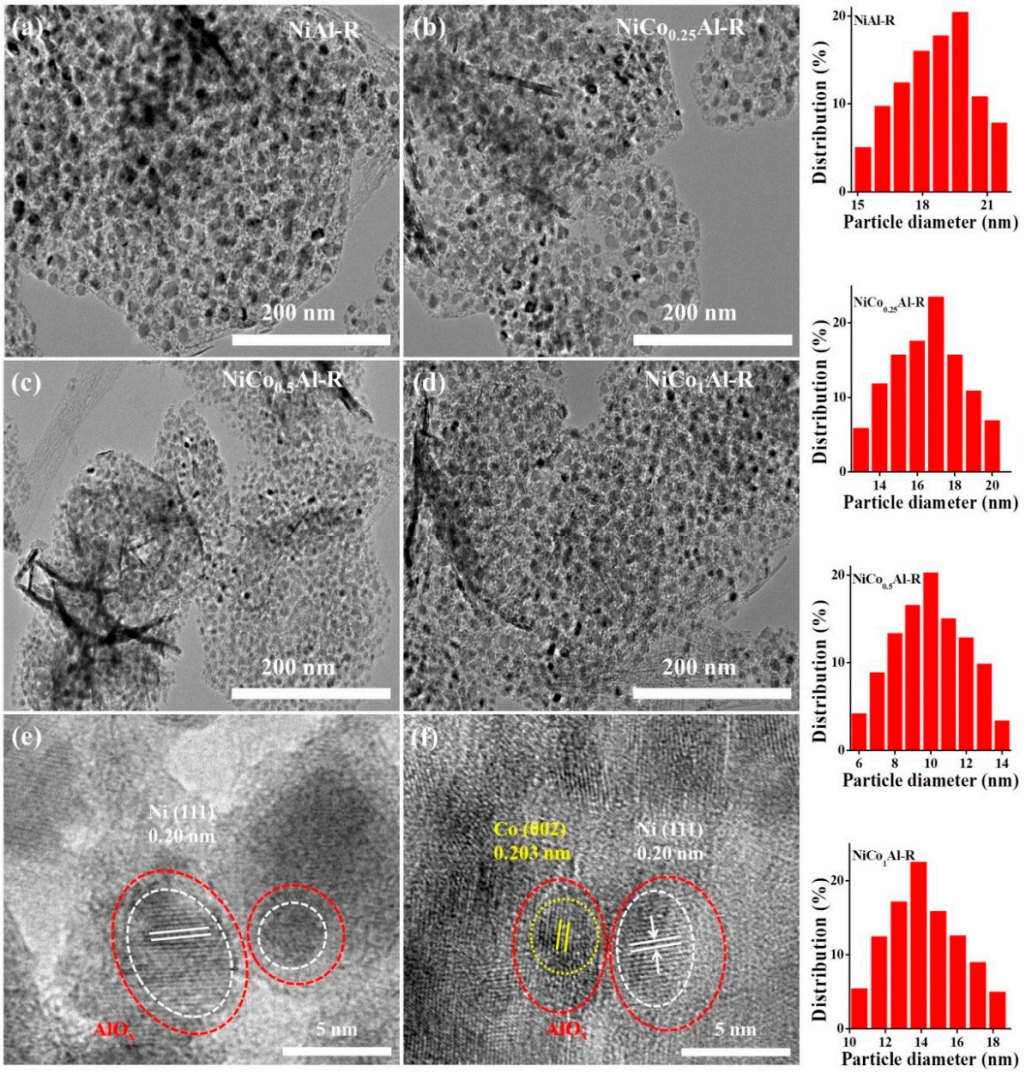

Figure 6. TEM images of $NiCo_x$Al-R catalysts: (**a**) NiAl-R, (**b**) $NiCo_{0.25}$Al-R, (**c**) $NiCo_{0.5}$Al-R, (**d**) $NiCo_1$Al-R, (**e**) NiAl-R and (**f**) $NiCo_{0.5}$Al-R. The histograms show the size distribution of Ni nanoparticles.

The spatial distribution of Ni, Co, Al and O in the $NiCo_{0.5}$Al-R catalyst was further studied by TEM-EDS mapping (shown in Figure 7). It can be found from Figure 7b that Al and O elements are mainly distributed around the Ni element, which is the same as the TEM results (shown in Figure 6e–f). Furthermore, the Co-promoter is uniformly dispersed in the $NiCo_{0.5}$Al-R catalyst. TEM-EDS mapping results show that the Co-promoted Ni-based catalysts prepared by direct reduction of hydrotalcites have a higher degree of dispersion, which is beneficial to improve the methanation activity of the catalysts.

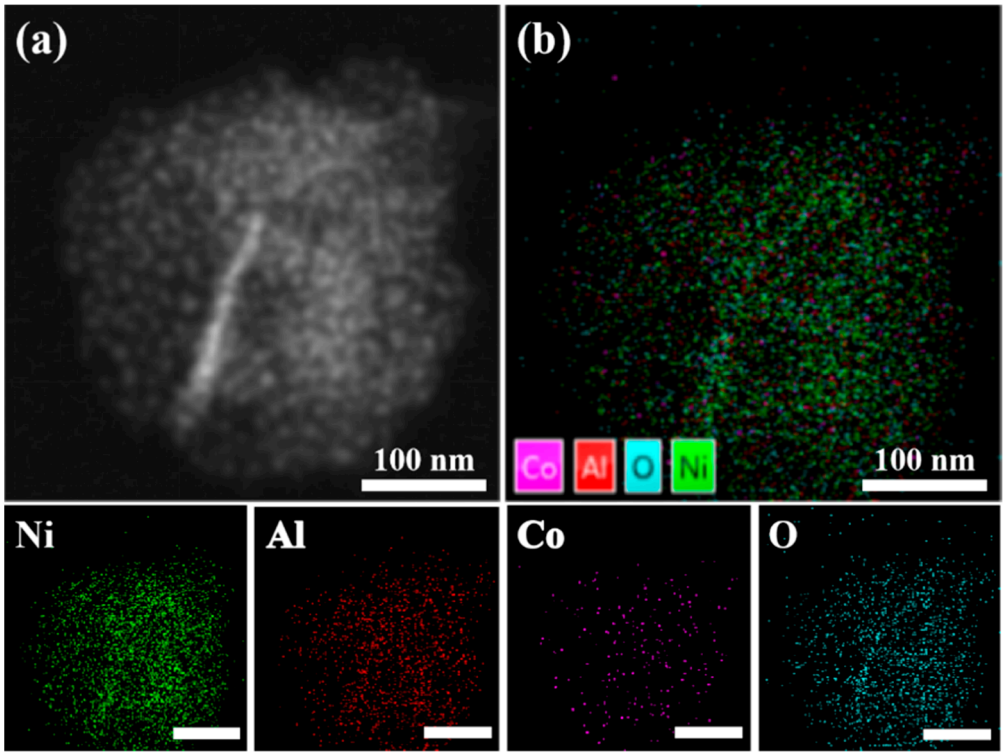

Figure 7. TEM image (**a**) and EDS mapping (**b**) of the $NiCo_{0.5}Al$-R catalyst.

2.2. Catalytic Activity Tests

In order to study the effect of Co on the low-temperature catalytic activity of Ni-based catalysts, we tested the catalytic performance of $NiCo_xAl$-R catalysts with CO_2 methanation as a probe reaction (shown in Figure 8a–c, 0.1 MPa, GHSV = 30,000 $mL \cdot g^{-1} \cdot h^{-1}$). When the reaction temperature reaches 250 °C, the conversion of CO_2 on the $NiCo_{0.5}Al$-R catalyst reaches 81%, but at this time, the conversion of CO_2 on the NiAl-R catalyst is only 26%. The reason why the low-temperature catalytic activity of $NiCo_{0.5}Al$-R catalyst is significantly improved is that the Co-promoter reduces the size of Ni nanoparticles in the catalyst (shown in Figures 1b and 6) and increases the number of moderately basic sites (shown in Figure 5). At the same time, the results also show that the smaller the size of the Ni particles, the more active sites are exposed, and therefore, the higher the activity of the catalyst, which is consistent with the results reported in the literature [50]. It can be seen from Figure 8a that the low-temperature catalytic performance of $NiCo_1Al$-R catalyst is lower than that of $NiCo_{0.5}Al$-R catalyst, which may be caused by the excessive Co covering part of the active sites of Ni. The performance test results of the catalysts also showed that no Co-NiO_x intermediate was formed during the reaction. This is inconsistent with the results reported in the literature due to the absence of oxygen in the CO_2 methanation reaction [51,52]. Therefore, although the auxiliary Co is added, the Co-NiO_x intermediate will not be formed during the CO_2 methanation reaction. In summary, doping with an appropriate amount of Co can significantly improve the low-temperature catalytic performance of the Ni-based catalyst, thereby reducing its activation temperature in the CO_2 methanation reaction.

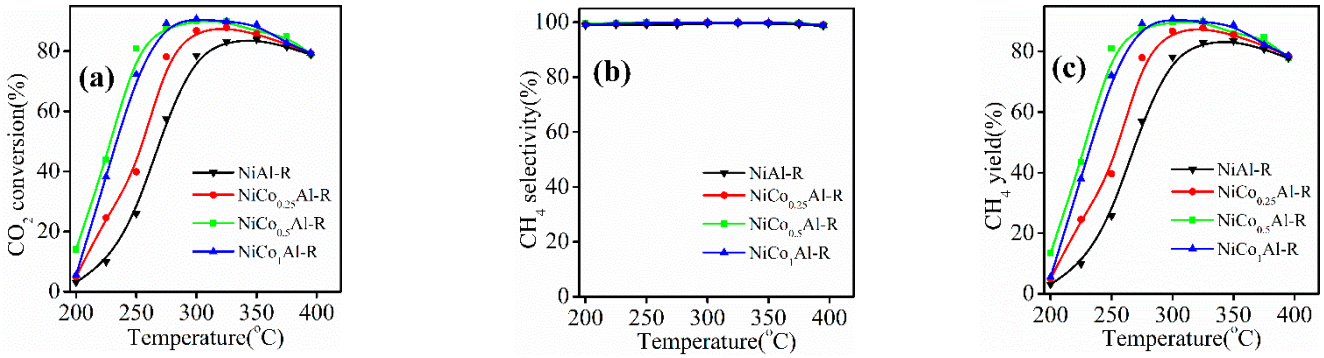

Figure 8. Catalytic performances of $NiCo_xAl$-R for CO_2 methanation: (**a**) CO_2 conversion, (**b**) CH_4 selectivity, (**c**) CH_4 yield.

Since the methanation of CO_2 is a strong exothermic reaction, an excellent nickel-based catalyst must not only have high low-temperature catalytic activity but also high stability. In view of this, we tested the stability of the $NiCo_{0.5}Al$-R catalyst at 300 °C (0.1 MPa, GHSV = 30,000 $mL \cdot g^{-1} \cdot h^{-1}$) (shown in Figure 9). The $NiCo_{0.5}Al$-R catalyst performance degradation at the beginning of the life test experiment is because the CO_2 methanation reaction has not reached a stable state. The stability test result showed that the $NiCo_{0.5}Al$-R catalyst still did not deactivate after 92 h of continuous reaction, which was attributed to the confinement effect of the AlO_x substrate on the Ni nanoparticles.

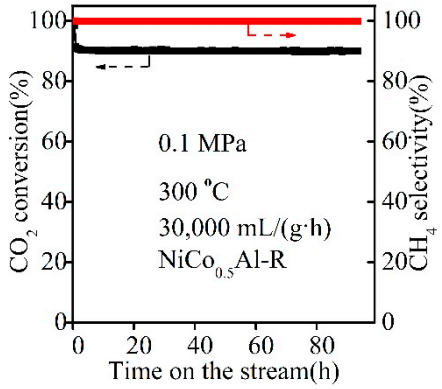

Figure 9. Stability test of the $NiCo_{0.5}Al$-R catalyst.

In order to study the change of Ni nanoparticle size and carbon deposit on the surface of the catalyst after the life test, we performed XRD and Raman tests on the catalyst after the reaction (shown in Figure 10a,b). The diffraction peaks at 44.6°, 51.9° and 76.8° correspond to the (111), (200) and (220) crystal planes of Ni [42], and the weak broad diffraction peaks located at 37.1° and 63.3° are attributed to the (111) and (220) crystal planes of NiO (fcc), respectively [53]. By comparing the XRD results of the catalyst before and after the stability test, it was found that the intensity and half-width of the characteristic diffraction peaks of Ni did not change significantly. This indicates that the size of Ni nanoparticles in the $NiCo_{0.5}Al$-R catalyst did not change significantly after the stability test. Additionally, through the TEM photograph of the $NiCo_{0.5}Al$-R catalyst after the reaction, it can be seen more clearly that there is no agglomeration of Ni particles (shown in Figure 11a). The average size of Ni particles in the $NiCo_{0.5}Al$-R catalyst after the reaction is 10.3 nm, which is basically the same as the size of Ni particles in the fresh catalyst (shown in Figure 6). Moreover, the XRD result of the $NiCo_{0.5}Al$-R used does not show the diffraction peaks of carbon species, which indicates that there is no carbon deposit on the catalyst surface or the amount of carbon deposit is too small to be detected. Raman spectroscopy was used to further confirm whether carbon deposits are formed. The Raman spectroscopy test results of the catalyst also do not find the signal peak of carbon material, which indicates that

there is no carbon deposit on the surface of the catalyst. Combining the XRD results and Raman results of the catalyst after the stability test shows that the catalyst has high stability and carbon deposition resistance.

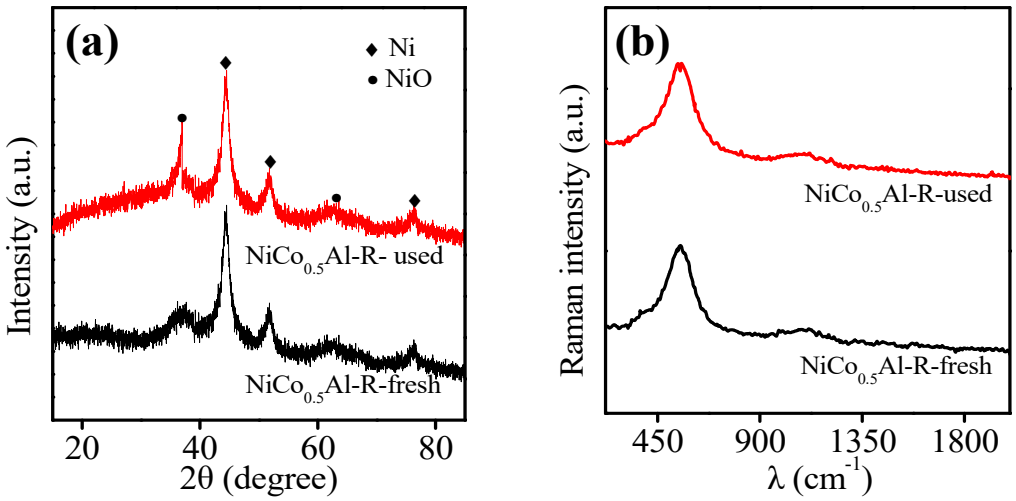

Figure 10. XRD patterns (**a**) and Raman spectrum (**b**) of $NiCo_{0.5}$Al-R-fresh and $NiCo_{0.5}$Al-R-used catalysts.

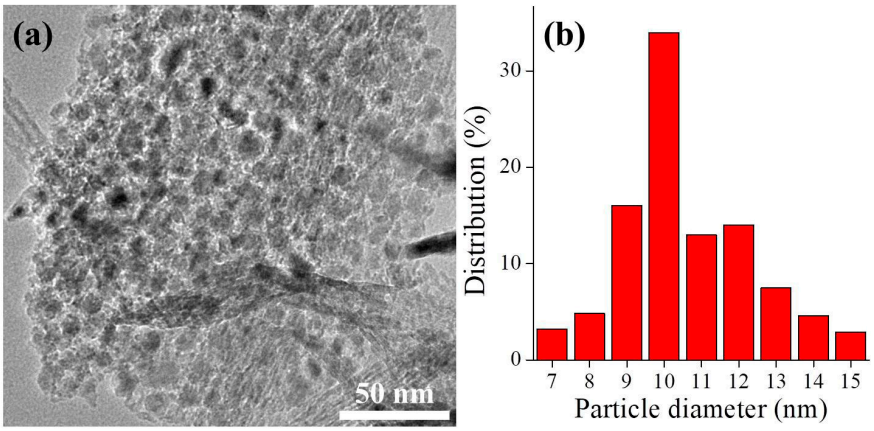

Figure 11. TEM (**a**) and particle size distribution (**b**) of the $NiCo_{0.5}$Al-R-used catalyst.

3. Materials and Methods

3.1. Chemicals

Chemical reagents involving Ni $(NO_3)_2{\cdot}6H_2O$, Co $(NO_3)_2{\cdot}9H_2O$, Al $(NO_3)_3{\cdot}9H_2O$ and urea $(CO(NH_2)_2)$ were provided by Zhengzhou Liyan Co. Ltd., in China. The reagents used in the experiment are of analytical grade, and no further purification is required.

3.2. Catalyst Preparation

The different molar ratios of $NiCo_x$Al-LDHs (x = 0, 0.25, 0.5, 1, Ni^{2+}/Al^{3+} = 2) were obtained by the hydrothermal method. Firstly, 10 mmol Ni $(NO_3)_2{\cdot}6H_2O$, Co $(NO_3)_2{\cdot}9H_2O$ and 5 mmol Al $(NO_3)_3{\cdot}9H_2O$ were dissolved in deionized water, for which the molar amounts of Co were 0, 0.25, 0.5 and 1 mmol. Secondly, 50 mmol of $CO(NH_2)_2$ precipitant was added. Then, the suspension solution was transferred to an autoclave heating for 12 h (120 °C). After the hydrothermal reaction, the obtained samples were filtered and centrifuged (8000 rpm) until the filtrate PH = 7. Finally, the samples were dried overnight at 80 °C. When the molar amount of Co was 0, 0.25, 0.5 and 1 mmol, the corresponding products were named NiAl-LDH, $NiCo_{0.25}$Al-LDH, $NiCo_{0.5}$Al-LDH and $NiCo_1$Al-LDH,

respectively. The catalysts were obtained by the reduction of LDH precursor in a pure H_2 atmosphere (600 °C, 2 h), denoted as NiAl-R, $NiCo_{0.25}$Al-R, $NiCo_{0.5}$Al-R and $NiCo_1$Al-R, respectively (R represents reduction).

3.3. Catalyst Characterization

X-ray diffraction equipment was used to characterize the phase composition of the samples. The test voltage of the equipment was 40 kV, and the current was 40 mA. The scanning speed was $10^\circ \cdot min^{-1}$ with the angle from 5° to 90° (2 θ).

For N_2 physisorption measurements, a Quantachrome NOVA 3200e (Quantachrome Corporation, Boynton Beach, FL, USA) was applied to determine the adsorption and desorption isotherm results.

The H_2-TPR and CO_2-TPD results of the catalysts were detected by a Quantachrome automatic chemical adsorption analyzer. In order to improve the accuracy of the H_2-TPR test results, we first heated the $NiCo_x$Al-LDHs to 150 °C in Ar atmosphere, followed by a temperature reduction to 50 °C, and finally heated it to 800 °C in 10%-H_2/Ar atmosphere and recorded data. For CO_2-TPD characterization, firstly, $NiCo_x$Al-LDHs (100 mg) were reduced in a H_2 atmosphere (600 °C, 2 h), and then the temperature dropped to 50 °C under the protection of Ar atmosphere. Immediately after the reduction, the sample was adsorbed for CO_2. After the adsorption was saturated, the temperature was raised, and the CO_2 desorption amount was recorded with the instrument.

The morphology and microstructure of the $NiCo_x$Al-LDHs precursors and $NiCo_x$Al-R catalysts were characterization by SEM (JSM-7001F, INCA X-MAX, Tokyo, Japan) and TEM (JEM-2010F, Tokyo, Japan).

Raman characterization was conducted on a Renishaw RM 2000 (λ = 532 nm, London, UK).

3.4. Catalytic Experiments

First of all, 0.05 g $NiCo_x$Al-R catalyst with 80–120 mesh was loaded in the fixed bed equipment. Then, the reduction mixture gases comprising H_2 and Ar (H_2/Ar = 1/9, V/V) were inserted, and the temperature was raised from 30 to 200 °C. Feed gases were then introduced, for which the composition was H_2, CO_2 and Ar (H_2/CO_2/Ar = 4/1/5). The reaction condition was T = 200–395 °C, p = 0.1 MPa and GHSV = 30,000 $mL \cdot g^{-1} \cdot h^{-1}$. The values of CO_2 and produced CO and CH_4 were measured using a gas chromatograph at each temperature after 1 h when the reaction reached steady state. The CO_2 conversion and CH_4 selectivity were calculated according to the following formula:

$$CO_2 \text{ conversion } (\%) = \frac{F_{CO_{2,in}} - F_{CO_{2,out}}}{F_{CO_{2,in}}} \times 100\%$$

$$CH_4 \text{ selectivity } (\%) = \frac{F_{CH_{4,out}}}{F_{CO_{2,in}} - F_{CO_{2,out}}} \times 100\%$$

where $F_{CO_{2,in}}$ is the flow rate of reactant CO_2; $F_{CO_{2,out}}$ and $F_{CH_{4,out}}$ represent the flow rate of CO_2 and CH_4 in the outlet.

4. Conclusions

In summary, in order to improve the low-temperature catalytic performance of the Ni-based catalysts in the CO_2 methanation reaction, Co-promoted Ni-based catalysts were successfully prepared by in situ reduction of $NiCo_x$Al-LDHs precursors. The results of CO_2-TPD and TEM prove that the Co assistant can regulate the number of moderately basic sites and the size of Ni nanoparticles in the Ni-based catalyst. Furthermore, the confinement effect of the AlO_x substrate effectively inhibits the migration and agglomeration of Ni particles during the reaction and improves the stability of the catalyst. The experimental results show that the $NiCo_{0.5}$Al-R catalyst has high low temperature catalytic performance, high stability and excellent carbon deposition resistance. Therefore, it has promising industrial application prospects.

Author Contributions: Conceptualization, F.Z. and P.S.; methodology, F.Z.; validation, F.Z., B.L. and P.S.; investigation, F.Z., B.L. and P.S.; resources, P.S.; writing—original draft preparation, F.Z., B.L. and P.S.; writing—review and editing, F.Z., B.L. and P.S.; supervision, P.S.; funding acquisition, P.S. All authors have read and agreed to the published version of the manuscript.

Funding: This work was supported by the National Key R&D Program of China (2018YFB0604504).

Institutional Review Board Statement: Not applicable.

Informed Consent Statement: Not applicable.

Data Availability Statement: Data available within the article.

Conflicts of Interest: There are no conflict of interest to declare.

References

1. Wang, Y.; Huang, H.; Zhang, Z.; Wang, C.; Yang, Y.; Li, Q.; Xu, D. Lead-free perovskite $Cs_2AgBiBr_6$@g-C_3N_4 Z-scheme system for improving CH_4 production in photocatalytic CO_2 reduction. *Appl. Catal. B* **2021**, *282*, 119570. [CrossRef]
2. Chaturvedi, K.R.; Ravilla, D.; Kaleem, W.; Jadhawar, P.; Sharma, T. Impact of low salinity water injection on CO_2 storage and oil Recovery for improved CO_2 utilization. *Chem. Eng. Sci.* **2021**, *229*, 116127. [CrossRef]
3. Wang, Z.; Huang, L.; Reina, T.; Efstathiou, A.; Wang, Q. Aqueous miscible organic LDH derived Ni-based catalysts for efficient CO_2 methanation. *Catalysts* **2020**, *10*, 1168. [CrossRef]
4. Spring, A.; Ilyina, T.; Marotzke, J. Inherent uncertainty disguises attribution of reduced atmospheric CO_2 growth to CO_2 emission reductions for up to a decade. *Environ. Res. Lett.* **2020**, *15*, 114058. [CrossRef]
5. Ishida, H.; Machan, C.; Robert, M.; Iwasawa, N. Editorial: Molecular catalysts for CO_2 fixation/reduction. *Front. Chem.* **2020**, *8*, 59. [CrossRef]
6. Rafiee, A. Modelling and optimization of methanol synthesis from hydrogen and CO_2. *J. Environ. Chem. Eng.* **2020**, *8*, 104314. [CrossRef]
7. Duyar, M.S.; Tsai, C.; Snider, J.L.; Singh, J.A.; Gallo, A.; Yoo, J.S.; Medford, A.J.; Abild-Pedersen, F.; Studt, F.; Kibsgaard, J.; et al. A highly active molybdenum phosphide catalyst for methanol synthesis from CO and CO_2. *Angew. Chem. Int. Ed. Engl.* **2018**, *57*, 15045–15050. [CrossRef]
8. Burger, T.; Donaubauer, P.; Hinrichsen, O. On the kinetics of the co-methanation of CO and CO_2 on a co-precipitated Ni-Al catalyst. *Appl. Catal. B* **2021**, *282*, 119408. [CrossRef]
9. Lehtinen, T.; Virtanen, H.; Santala, S.; Santala, V. Production of alkanes from CO_2 by engineered bacteria. *Biotechnol. Biofuels* **2018**, *11*, 228. [CrossRef] [PubMed]
10. Xing, S.; Lv, P.; Yuan, H.; Yang, L.; Wang, Z.; Yuan, Z.; Chen, Y. Insight into forced hydrogen re-arrangement and altered reaction pathways in a protocol for CO_2 catalytic processing of oleic acid into C_8–C_{15} alkanes. *Green Chem.* **2017**, *19*, 4157–4168. [CrossRef]
11. Ghaib, K.; Nitz, K.; Ben-Fares, F.Z. Chemical methanation of CO_2: A review. *ChemBioEng Rev.* **2016**, *3*, 266–275. [CrossRef]
12. Ghasemi, M.; Mohammadi, M.; Sedighi, M. Sustainable production of light olefins from greenhouse gas CO_2 over SAPO-34 supported modified cerium oxide. *Microporous Mesoporous Mater.* **2020**, *297*, 110029. [CrossRef]
13. Ding, J.; Zhao, W.; Zi, L.; Xu, X.; Liu, Q.; Zhong, Q.; Xu, Y. Promotional effect of ZrO_2 on supported FeCoK catalysts for ethylene synthesis from catalytic CO_2 hydrogenation. *Int. J. Hydrogen Energy* **2020**, *45*, 15254–15262. [CrossRef]
14. Huang, J.; Wang, W.; Fei, Z.; Liu, Q.; Chen, X.; Zhang, Z.; Tang, J.; Cui, M.; Qiao, X. Enhanced light olefin production in chloromethane coupling over Mg/Ca modified durable HZSM-5 catalyst. *Ind. Eng. Chem. Res.* **2019**, *58*, 5131–5139. [CrossRef]
15. Siudyga, T.; Kapkowski, M.; Janas, D.; Wasiak, T.; Sitko, R.; Zubko, M.; Szade, J.; Balin, K.; Klimontko, J.; Lach, D.; et al. Nano-Ru supported on Ni nanowires for low-temperature carbon dioxide methanation. *Catalysts* **2020**, *10*, 513. [CrossRef]
16. Siudyga, T.; Kapkowski, M.; Bartczak, P.; Zubko, M.; Szade, J.; Balin, K.; Antoniotti, S.; Polanski, J. Ultra-low temperature carbon (di)oxide hydrogenation catalyzed by hybrid ruthenium–nickel nanocatalysts: Towards sustainable methane production. *Green Chem.* **2020**, *22*, 5143–5150. [CrossRef]
17. Zhang, Z.; Xiao, Q.; Gu, J. Effective synthesis of zeolite encapsulated Ni nanoparticles with excellent catalytic performance for hydrogenation of CO_2 to CH_4. *Dalton Trans.* **2020**, *49*, 14771–14775. [CrossRef]
18. Zeng, L.; Wang, Y.; Li, Z.; Song, Y.; Zhang, J.; Wang, J.; He, X.; Wang, C.; Lin, W. Highly dispersed Ni catalyst on metal-organic framework-derived porous hydrous zirconia for CO_2 methanation. *ACS Appl. Mater. Interfaces* **2020**, *12*, 17436–17442. [CrossRef]
19. Kikkawa, S.; Teramura, K.; Asakura, H.; Hosokawa, S.; Tanaka, T. Ni–Pt alloy nanoparticles with isolated Pt atoms and their cooperative neighboring Ni atoms for selective hydrogenation of CO_2 toward CH_4 evolution: In situ and transient fourier transform infrared studies. *ACS Appl. Nano Mater.* **2020**, *3*, 9633–9644. [CrossRef]
20. Han, D.; Kim, Y.; Byun, H.; Cho, W.; Baek, Y. CO_2 methanation of biogas over 20 wt% Ni-Mg-Al catalyst: On the effect of N_2, CH_4, and O_2 on CO_2 conversion rate. *Catalysts* **2020**, *10*, 1201. [CrossRef]
21. Lu, B.; Zhuang, J.; Du, J.; Gu, F.; Xu, G.; Zhong, Z.; Liu, Q.; Su, F. Highly dispersed Ni nanocatalysts derived from NiMnAl-hydrotalcites as high-performing catalyst for low-temperature syngas methanation. *Catalysts* **2019**, *9*, 282. [CrossRef]

22. Mutz, B.; Carvalho, H.W.P.; Mangold, S.; Kleist, W.; Grunwaldt, J.D. Methanation of CO_2: Structural response of a Ni-based catalyst under fluctuating reaction conditions unraveled by operando spectroscopy. *J. Catal.* **2015**, *327*, 48–53. [CrossRef]
23. Italiano, C.; Llorca, J.; Pino, L.; Ferraro, M.; Antonucci, V.; Vita, A. CO and CO_2 methanation over Ni catalysts supported on CeO_2, Al_2O_3 and Y_2O_3 oxides. *Appl. Catal. B* **2020**, *264*, 118494. [CrossRef]
24. Wang, W.; Duong-Viet, C.; Ba, H.; Baaziz, W.; Tuci, G.; Caporali, S.; Nguyen-Dinh, L.; Ersen, O.; Giambastiani, G.; Pham-Huu, C. Nickel nanoparticles decorated nitrogen-doped carbon nanotubes (Ni/N-CNT): A robust catalyst for the efficient and selective CO_2 methanation. *ACS Appl. Energy Mater.* **2018**, *2*, 1111–1120. [CrossRef]
25. Yan, X.; Zhao, B.; Liu, Y.; Li, Y. Dielectric barrier discharge plasma for preparation of Ni-based catalysts with enhanced coke resistance: Current status and perspective. *Catal. Today* **2015**, *256*, 29–40. [CrossRef]
26. Wolf, M.; Wong, L.H.; Schüler, C.; Hinrichsen, O. CO_2 methanation on transition-metal-promoted Ni-Al catalysts: Sulfur poisoning and the role of CO_2 adsorption capacity for catalyst activity. *J. CO_2 Util.* **2020**, *36*, 276–287. [CrossRef]
27. Quindimil, A.; De-La-Torre, U.; Pereda-Ayo, B.; González-Marcos, G.A.; González-Velasco, J.R. Ni catalysts with La as promoter supported over Y- and BETA- zeolites for CO_2 methanation. *Appl. Catal. B* **2018**, *238*, 393–403. [CrossRef]
28. Ahmad, W.; Younis, M.N.; Shawabkeh, R.; Ahmed, S. Synthesis of lanthanide series (La, Ce, Pr, Eu & Gd) promoted Ni/γ-Al_2O_3 catalysts for methanation of CO_2 at low temperature under atmospheric pressure. *Catal. Commun.* **2017**, *100*, 121–126.
29. Xu, L.; Wang, F.; Chen, M.; Zhang, J.; Yuan, K.; Wang, L.; Wu, K.; Xu, G.; Chen, W. CO_2 methanation over a Ni based ordered mesoporous catalyst for the production of synthetic natural gas. *RSC Adv.* **2016**, *6*, 28489–28499. [CrossRef]
30. Abate, S.; Mebrahtu, C.; Giglio, E.; Deorsola, F.; Bensaid, S.; Perathoner, S.; Pirone, R.; Centi, G. Catalytic Performance of γ-Al_2O_3–ZrO_2–TiO_2–CeO_2 composite oxide supported Ni-based catalysts for CO_2 methanation. *Ind. Eng. Chem. Res.* **2016**, *55*, 4451–4460. [CrossRef]
31. Huang, X.; Wang, P.; Zhang, Z.; Zhang, S.; Du, X.; Bi, Q.; Huang, F. Efficient conversion of CO_2 to methane using thin-layer SiO_x matrix anchored nickel catalysts. *New J. Chem.* **2019**, *43*, 13217–13224. [CrossRef]
32. Zhu, P.; Chen, Q.; Yoneyama, Y.; Tsubaki, N. Nanoparticle modified Ni-based bimodal pore catalysts for enhanced CO_2 methanation. *RSC Adv.* **2014**, *4*, 64617–64624. [CrossRef]
33. Frontera, P.; Macario, A.; Monforte, G.; Bonura, G.; Ferraro, M.; Dispenza, G.; Antonucci, V.; Aricò, A.S.; Antonucci, P.L. The role of gadolinia doped ceria support on the promotion of CO_2 methanation over Ni and NiFe catalysts. *Int. J. Hydrogen Energy* **2017**, *42*, 26828–26842. [CrossRef]
34. Huang, T.J.; Yu, T.C. Effect of steam and carbon dioxide pretreatments on methane decomposition and carbon gasification over doped-ceria supported nickel catalyst. *Catal. Lett.* **2005**, *102*, 175–181. [CrossRef]
35. Zhang, F.; Lu, B.; Sun, P. Highly stable Ni-based catalysts derived from LDHs supported on zeolite for CO_2 methanation. *Int. J. Hydrogen Energy* **2020**, *45*, 16183–16192. [CrossRef]
36. Wang, K.; Zhang, L.; Su, Y.; Shao, D.; Zeng, S.; Wang, W. Photoreduction of carbon dioxide of atmospheric concentration to methane with water over CoAl-layered double hydroxide nanosheets. *J. Mater. Chem. A* **2018**, *6*, 8366–8373. [CrossRef]
37. Chen, G.; Gao, R.; Zhao, Y.; Li, Z.; Waterhouse, G.I.N.; Shi, R.; Zhao, J.; Zhang, M.; Shang, L.; Sheng, G.; et al. Alumina-supported CoFe alloy catalysts derived from layered-double-hydroxide nanosheets for efficient photothermal CO_2 hydrogenation to hydrocarbons. *Adv. Mater.* **2018**, *30*, 1704663. [CrossRef]
38. Martins, J.A.; Faria, A.C.; Soria, M.A.; Miguel, C.V.; Rodrigues, A.E.; Madeira, L.M. CO_2 methanation over hydrotalcite-derived nickel/ruthenium and supported ruthenium catalysts. *Catalysts* **2019**, *9*, 1008. [CrossRef]
39. Mebrahtu, C.; Krebs, F.; Perathoner, S.; Abate, S.; Centi, G.; Palkovits, R. Hydrotalcite based Ni-Fe/(Mg, Al)O_x catalysts for CO_2 methanation-tailoring Fe content for improved CO dissociation, basicity, and particle size. *Catal. Sci. Technol.* **2018**, *8*, 1016–1027. [CrossRef]
40. Aider, N.; Touahra, F.; Bali, F.; Djebarri, B.; Lerari, D.; Bachari, K.; Halliche, D. Improvement of catalytic stability and carbon resistance in the process of CO_2 reforming of methane by CoAl and CoFe hydrotalcite-derived catalysts. *Int. J. Hydrog. Energy* **2018**, *43*, 8256–8266. [CrossRef]
41. Wierzbicki, D.; Baranc, R.; Dębeka, R.; Motaka, M.; Gálvezb, M.E.; Grzybeka, T.; Costab, P.D.; Glatzelc, P. Examination of the influence of La promotion on Ni state in hydrotalcite derived catalysts under CO_2 methanation reaction conditions operando X-ray absorption and emission spectroscopy investigation. *Appl. Catal. B* **2018**, *232*, 409–419. [CrossRef]
42. Tada, S.; Shimizu, T.; Kameyama, H.; Haneda, T.; Kikuchi, R. Ni/CeO_2 catalysts with high CO_2 methanation activity and high CH_4 selectivity at low temperatures. *Int. J. Hydrog. Energy* **2012**, *37*, 5527–5531. [CrossRef]
43. Tang, G.; Gong, D.; Liu, H.; Wang, L. Highly loaded mesoporous Ni–La_2O_3 catalyst prepared by colloidal solution combustion method for CO_2 methanation. *Catalysts* **2019**, *9*, 442. [CrossRef]
44. Hou, Z.; Yashima, T. Supported Co catalysts for methane reforming with CO_2. *React. Kinet. Catal. Lett.* **2004**, *81*, 153–159. [CrossRef]
45. Liotta, L.F.; Di Carlo, G.; Pantaleo, G.; Venezia, A.M.; Deganello, G. Co_3O_4/CeO_2 composite oxides for methane emissions abatement: Relationship between Co_3O_4-CeO_2 interaction and catalytic activity. *Appl. Catal. B* **2006**, *66*, 217–227. [CrossRef]
46. Konsolakis, M.; Carabineiro, S.A.C.; Marnellos, G.E.; Asad, M.F.; Soares, O.; Pereira, M.F.R.; Orfao, J.J.M.; Figueiredo, J.L. Effect of cobalt loading on the solid state properties and ethyl acetate oxidation performance of cobalt-cerium mixed oxides. *J. Colloid Interface Sci.* **2017**, *496*, 141–149. [CrossRef]
47. Jia, X.; Zhang, X.; Rui, N.; Hu, X.; Liu, C.J. Structural effect of Ni/ZrO_2 catalyst on CO_2 methanation with enhanced activity. *Appl. Catal. B* **2019**, *244*, 159–169. [CrossRef]

48. Liang, C.; Zhang, L.; Zheng, Y.; Zhang, S.; Liu, Q.; Gao, G.; Dong, D.; Wang, Y.; Xu, L.; Hu, X. Methanation of CO_2 over nickel catalysts: Impacts of acidic/basic sites on formation of the reaction intermediates. *Fuel* **2020**, *262*, 116521. [CrossRef]
49. Liu, J.; Cao, A.; Si, J.; Zhang, L.; Hao, Q.; Liu, Y. Nanoparticles of Ni-Co alloy derived from layered double hydroxides and their catalytic performance for CO methanation. *Nano* **2016**, *11*, 1650118. [CrossRef]
50. Choi, H.; Oh, S.; Tran, S.B.T.; Park, J.Y. Size-controlled model Ni catalysts on Ga_2O_3 for CO_2 hydrogenation to methanol. *J. Catal.* **2019**, *376*, 68–76. [CrossRef]
51. Wu, C.H.; Liu, C.; Su, D.; Xin, H.L.; Fang, H.T.; Eren, B.; Zhang, S.; Murray, C.B.; Salmeron, M.B. Bimetallic synergy in cobalt-palladium nanocatalysts for CO oxidation. *Nat. Catal.* **2018**, *2*, 78–85. [CrossRef]
52. Kim, T.S.; Kim, J.; Song, H.C.; Kim, D.; Jeong, B.; Lee, J.; Shin, J.W.; Ryoo, R.; Park, J.Y. Catalytic synergy on PtNi bimetal catalysts driven by interfacial intermediate structures. *ACS Catal.* **2020**, *10*, 10459–10467. [CrossRef]
53. Fan, Q.; Li, X.; Yang, Z.; Han, J.; Xu, S.; Zhang, F. Double-confined nickel nanocatalyst derived from layered double hydroxide precursor: Atomic scale insight into microstructure evolution. *Chem. Mater.* **2016**, *28*, 6296–6304. [CrossRef]